© Universiti Tun Hussein Onn Malaysia Publisher's Office

IJIE

http://penerbit.uthm.edu.my/ojs/index.php/ijie
ISSN : 2229-838X e-ISSN : 2600-7916

The International Journal of Integrated Engineering

Focal Region Ray Tracing of Conventional and Shaped Lens Antenna

M. Muhsin[1,2], Kamilia Kamardin[1*], Yoshihide Yamada[1]

[1]Malaysia-Japan International Institute of Technology,
Universiti Teknologi Malaysia, Kuala Lumpur, 54100, MALAYSIA

[2]Department of Telecommunication Engineering,
Institut Teknologi Telkom Surabaya, Surabaya, 60231, INDONESIA

*Corresponding Author

DOI: https://doi.org/10.30880/ijie.2023.15.03.013
Received 6 November 2022; Accepted 29 May 2023; Available online 15 August 2023

Abstract: Multibeam lens antennas are useful for 5G mobile communication systems. For multibeam design, feed position determination of specified lens becomes an important subject. The feed position data can be obtained from focal region ray tracing. In this paper, a simple and convenient ray tracing method by using the MATLAB function of "polyxpoly" is proposed. To evaluate the program, focal region ray tracing on conventional hyperbolic planar, spherical convex, and Abbe's sine condition lens are presented in this paper. For focal region ray tracing, parallel incident ray is considered. The incident ray's angle is changed from 0 degree to 30 degrees with an interval of 10 degrees. On hyperbolic planar and spherical convex lenses, ray concentration at the focal region is distorted at incident angle of 10 degrees and above. On Abbe's sine condition lens, good concentration is maintained until 20 degrees. Concentration points agree well with the theoretical value. Therefore, the correctness of the program is ensured.

Keywords: Focal region, ray tracing, multibeam antenna, lens antenna

1. Introduction

At 5G mobile and beyond, new radio wave technologies such as millimeter wave, small cell, and multibeam base stations are introduced [1-7]. For multibeam technology, dielectric lens antennas are well known to have excellent multibeam radiation patterns [8-11]. Especially, the Abbe's sine condition lens is the most famous for excellent multibeam [11]. The feed positions of multibeam are theoretically given and focal regions are shown [12]. To apply multibeam lens antennas for 5G base station, many lens structures should be studied. Therefore, focal region ray tracing for arbitral lens shape is required.

Determination of feed position is important to achieve good multibeam performance [8, 13]. Focal region ray tracing provides useful data for feed position selection. The data is collected from tracing the ray of the lens from the opposite side, which is also called receiving mode. The data then can be analyzed to find the best feed position.

In this paper, a simple and convenient ray tracing method is proposed. It is programmed in MATLAB using the function of "polyxpoly" [14]. Refraction process is embedded within the program. Models of lenses are constructed on MATLAB by a group of discrete points representing lens surfaces. Then, receiving mode ray tracing is conducted. Incident rays are multiple parallel rays at specified angles. Then, ray tracing is conducted based on Snell's law and final refracted rays are obtained. The ray is then analyzed by finding focal points based on ray concentration. The found focal points and rays are then compared to evaluate characteristic and suitability of the lens shape for multibeam. Focal region

*Corresponding author: kamilia@utm.my

ray tracing of several lens shapes is presented. The presented lens shapes are hyperbolic planar lens, spherical convex lens, and Abbe's sine condition lens.

2. Lens Shaping

In this part, models of conventional lenses and shaped lens are presented. There 3 lenses are presented: hyperbolic planar lens, spherical convex lens, and Abbe's sine condition lens. Hyperbolic planar and spherical convex lenses are conventional lenses. Shape of these lenses are described by a simple equation. Abbe's sine condition lens is shaped lens which is based on the lens shaping method.

2.1 Conventional Lens

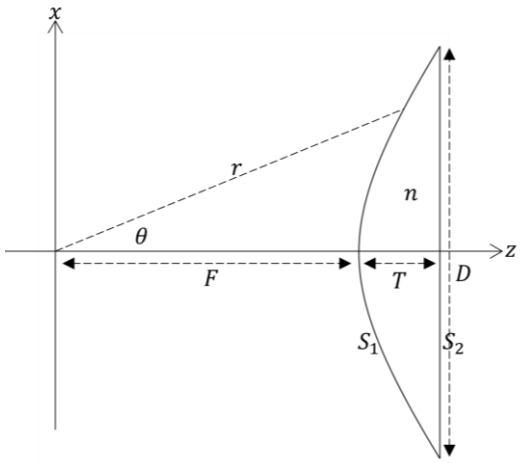

Fig, 1 - Hyperbolic planar lens

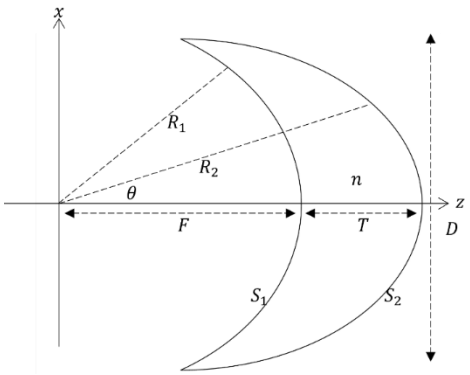

Fig. 2 - Spherical convex lens

Hyperbolic planar and spherical convex lens model are constructed in MATLAB. The model follows description of lens shape by simple equation. Fig. 1 and 2 show hyperbolic planar and spherical convex lens shape, respectively.

2.1.1 Hyperbolic Planar Lens

Inner surface of hyperbolic planar lens is [11]

$$r = \frac{(n-1)F}{n\cos(\theta) - 1} \tag{1}$$

where F is length and n is refractive index of the lens. Then, thickness of hyperbolic planar lens is

$$T = \frac{1}{n+1}\left[\sqrt{F^2 + \frac{(n+1)D^2}{4(n-1)}} - F\right] \tag{2}$$

Lens diameter is set to $D = 200$ mm. Then focal length is $F = 115.47$ mm.

2.1.2 Spherical Convex Lens

Inner surface of spherical convex lens is

$$R_1 = F \tag{3}$$

and outer surface of spherical convex lens is

$$R_2 = \frac{(n-1)(F+T)}{n - \cos\theta} \tag{4}$$

with thickness of spherical convex lens is

$$T = \frac{2F - \sqrt{4F^2 - D^2}}{2(n-1)}. \tag{5}$$

Lens diameter is set to $D = 200$ mm. Then focal length is $F = 115.47$ mm.

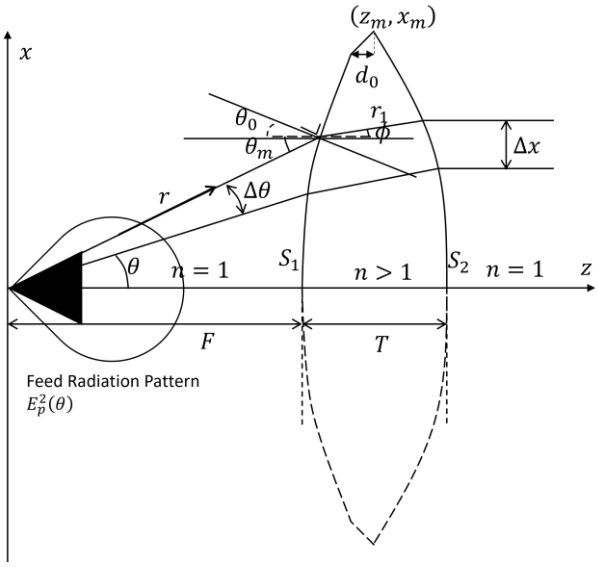

Fig. 3 - Concept of lens shaping

2.2 Shaped Lens

Abbe's sine lens is well known for good multibeam radiation pattern. It is designed as shaped lens following some condition described in equations. In this paper, Abbe's sine condition lens is constructed using MATLAB program based on the applied conditions. Structure of the lens is defined by a lens shaping method [11] as seen in Fig. 3. It follows some conditions and equations. The first is refraction of S_1 which defined by Snell's Law [15]

$$\frac{dr}{d\theta} = \frac{nr\sin(\theta - \phi)}{n\cos(\theta - \phi) - 1} \tag{6}$$

with n is refraction index of the lens. The second is Snell's Law on S_2

$$\frac{dz}{d\theta} = \frac{n\sin\phi}{1 - n\cos\phi}\frac{dx}{d\theta}. \tag{7}$$

The third is total path length of

$$L_t = r + nr_1 + Z_0 - Z \tag{8}$$

Where

$$r_1 = \frac{Z - r\cos\theta}{\cos\phi} \tag{9}$$

with Z_0 is the aperture plane position and Z is the distance of the inner surface at the edge to the aperture plane. The last equation is defined by Abbe's sine condition of [11]

$$\frac{dx}{d\theta} = F_s\cos\theta \tag{10}$$

as seen in Fig. 4.

The program works by sweeping θ from 0 to θ_m with the step of $\Delta\theta$ solving Equation (6), (7), (8), and (10). Some initial values need to be determined. These parameters are set to $\theta_m = 60°$, $\theta_0 = 35°$, $r_0 = 115.47$ mm, $d_0 = 0.0001$

mm, and $n = 2$. The output of the lens shaping program is used as a set of ray surfaces' discrete points for focal region ray tracing.

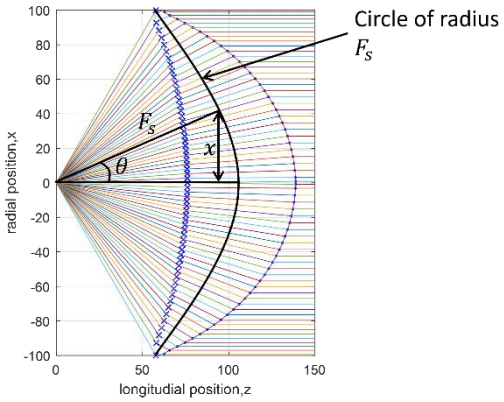

Fig. 4 - Abbe's sine condition lens

3. Focal Region Ray Tracing on MATLAB

Focal region ray tracing uses receiving mode from right to left (Area 3 to Area 1) is shown in Fig. 5. Incident parallel rays are generated in Area 3 with the gradient of $\tan\varphi_q$ and Δx gap on x-axis. Ray tracing is conducted for each. Refraction points on S_2 are named (z_b, x_b) and normal vector angle is θ_q. Snell's law is then applied to find the refracted ray in Area 2. Ray tracing is then continued by finding refraction points on S_1 which are named (z_a, x_a) and normal vector angle θ_q can be defined. Finally, refracted rays in Area 1 can be drawn. From two consecutive rays in Area 1, (z_f, x_f) can be found and the final refracted rays can be analyzed to find the best feed position.

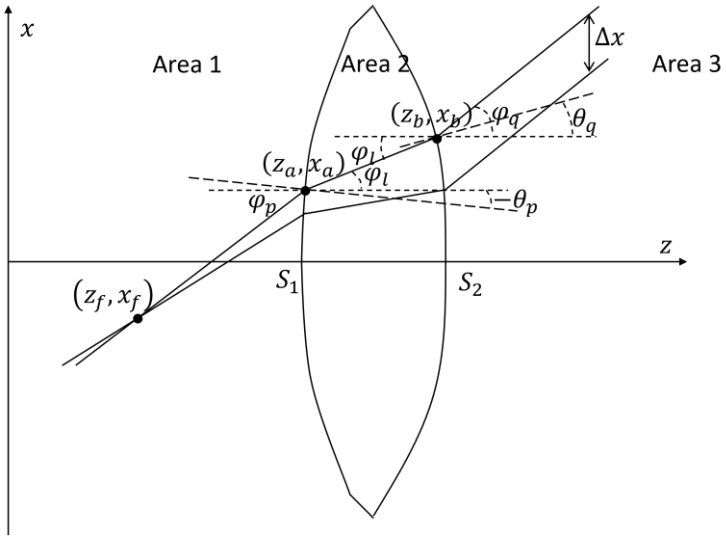

Fig. 5 - Concept of ray tracing on receiving mode

3.1 Finding Refraction Point on S_2

Curve S_2 is made by many discrete points from the result of lens shaping. Discrete points are then connected making the whole lens' shape. Incoming ray in Area 3 from (z_i, x_i) is then extended very far reaching the x-axis at $(0, x_e)$. Therefore, the function "polyxpoly" on MATLAB can find the intersection between curve S_2 and incoming ray in Area 3 as P_2 in Fig. 6. P_2 is then used as the refraction point on S_2.

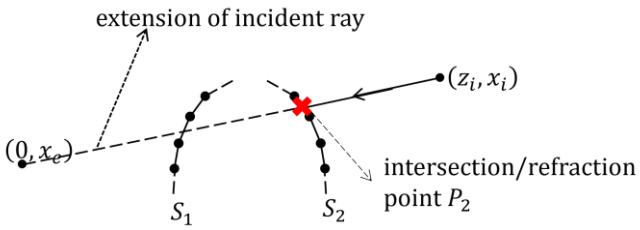

Fig. 6 - Finding intersection point on S_2

3.2 Finding Refraction Point on S_1

Normal vector angle of θ_q is calculated by a very accurate approximation from two nearest points with the refraction point (P_2) as shown in Fig. 7. Then, φ_l can be found by applying Snell's law [16] as

$$n = \frac{\sin(\varphi_q - \theta_q)}{\sin(\varphi_l - \theta_q)}. \tag{11}$$

After φ_l is obtained for all rays, rays inside lens can be drawn from the refraction points to the left direction (S_1) with the gradient of $\tan \varphi_l$ following linear line equation.

Similar with S_2, S_1 is made by many discrete points which connected. Straight line is drawn from P_2 and extended very far reaching x-axis at $(0, x_r)$ as shown in Fig. 7. Then, intersection P_1 between curve S_1 and the ray can be found using "polyxpoly" function. P_1 is then used as the refraction point on S_1.

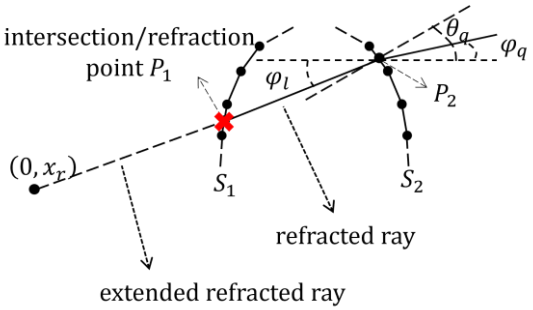

Fig. 7 - Finding intersection point on S_1

3.3 Focal Region Ray

Normal vector angle of θ_p is calculated by a very accurate approximation from two nearest points with the refraction point (P_1) as seen in Fig. 8. Then, φ_p can be found by applying Snell's law [16] as

$$n = \frac{\sin(\varphi_p - \theta_p)}{\sin(\varphi_l - \theta_p)}. \tag{12}$$

After φ_p is obtained for all rays, final rays can be drawn from P_1 with gradient of φ_p.

Similar with S_2, S_1 is made by many discrete points which connected. Straight line is drawn from P_2 and extended very far reaching x-axis at $(0, x_r)$. Then, intersection P_1 between curve S_1 and the ray can be found using "polyxpoly" function. P_1 is then used as the refraction point on S_1.

Final refracted rays on Area 1 are analyzed to find the estimated best feed position. This position can be defined by finding the most concentrated ray points. If the rays are very well concentrated, the feed position can be easily found with high conviction. Good concentration of rays also means that the lens can possibly provide good multibeam performance.

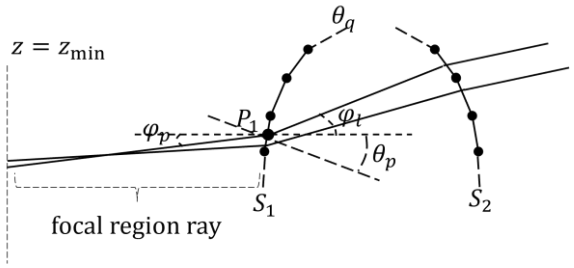

Fig. 8 - Focal region ray

4. Results and Discussions

4.1 Hyperbolic Planar Lens

a b

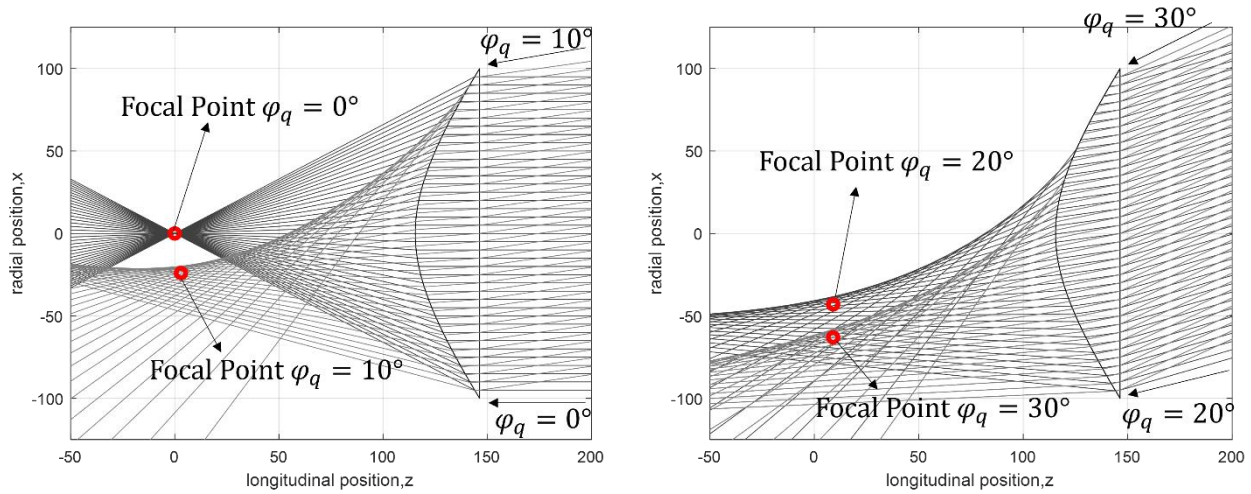

Fig. 8 - Results on hyperbolic planar lens (a) 0° and 10° incident angle; (b) 20° and 30° incident angle

Fig. 8 shows results of receiving mode ray tracing on hyperbolic planar lens and the estimated focal point for 0°, 10°, 20°, and 30° incident angle. For on-focus incident angle (0°), the rays are very concentrated at $(0,0)$. However, with the increase of incident angle, the ray become less concentrated. Then, for incident angle more than 10°, the total internal reflection (TIR) occurred. It makes difficulty to find focal point. From these results, good multibeam performance of this lens may not be expected.

4.2 Spherical Convex Lens

Fig. 9 shows results of receiving mode ray tracing on spherical convex lens and the estimated focal point for 0°, 10°, 20°, and 30° incident angle. For on-focus incident angle (0°), the rays are very concentrated at $(0,0)$. Similar with hyperbolic planar, with the increase of incident angle, the ray become less concentrated. However, concertation of ray is better compared to hyperbolic planar lens. Unlike hyperbolic planar lens, TIR is not shown for this lens shape. From these results, better multibeam performance of this lens may be expected compared to hyperbolic planar lens.

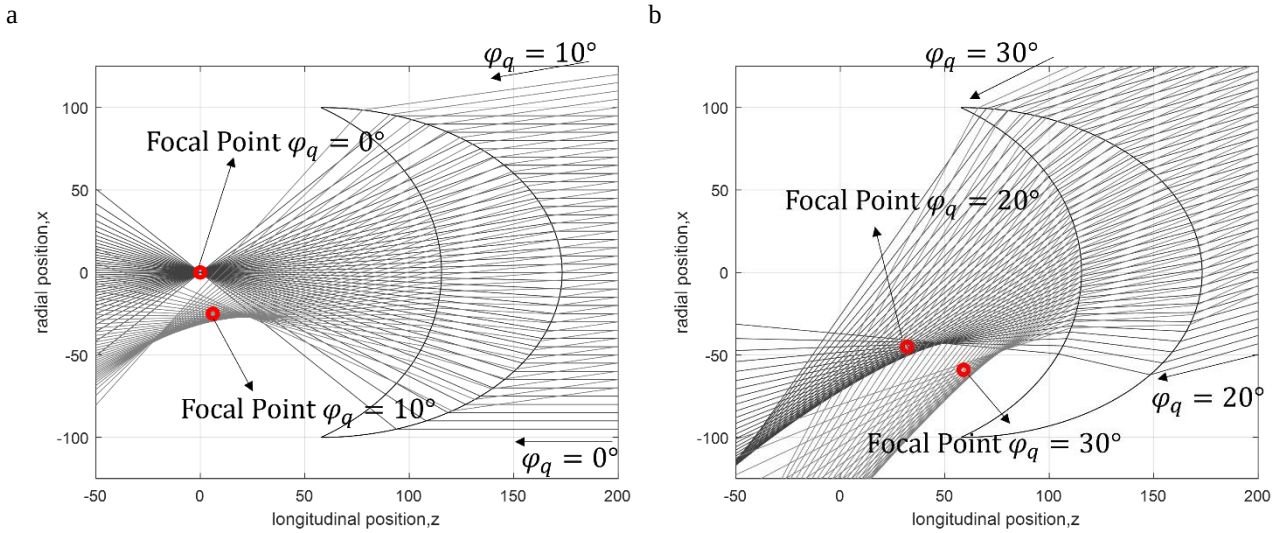

Fig. 9 - Results on spherical convex lens (a) 0° and 10° incident angle; (b) 20° and 30° incident angle

4.3 Abbe's Sine condition lens

Fig. 10 shows results of receiving mode ray tracing on Abbe's sine condition lens and the estimated focal point for 0°, 10°, 20°, and 30° incident angle. For on-focus incident angle (0°), the rays are very concentrated at $(0,0)$. For incident angle 10° and 20°, the rays are still well concentrated. Then, the rays become less concentrated at 30° incident angle. From these results, good multibeam performance of this lens may be expected. However, the less concentrated rays for high incident angle indicating that there will be some limitation of multibeam coverage, especially for high angle.

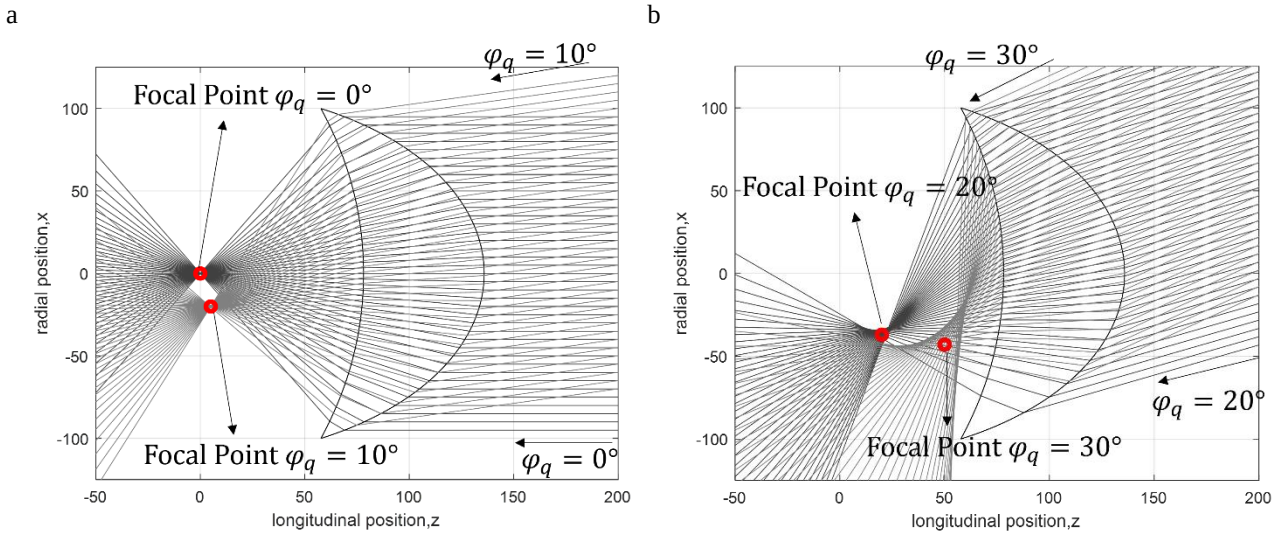

Fig. 10 - Results on Abbe's sine condition lens (a) 0° and 10° incident angle; (b) 20° and 30° incident angle

4.4 Comparison of Focal Point

Fig. 11 shows comparison of focal point on hyperbolic planar lens, spherical convex lens, and Abbe's sine condition lens. Focal point of Abbe's sine condition lens shows good agreement with the known locus of this lens shape. The locus is defined by radius of [12]

$$r = f_s \cos^2 \theta \tag{13}$$

from $(f_s, 0)$ which can be derived as

$$x = f_s \cos^2 \theta \sin \theta \tag{14}$$

And

$$z = f_s - f_s \cos^3 \theta \tag{15}$$

with $f_s = R/\sin 60°$ is equivalent focal length of the lens. This good agreement proves that the method is valid. Then, for hyperbolic planar and spherical convex lens, locus has lower bend compared to Abbe's sine condition lens. Locus of spherical convex lens is smooth and close to Abbe's locus. However, locus of hyperbolic planar lens is less smooth due to some TIR occurred at high angle.

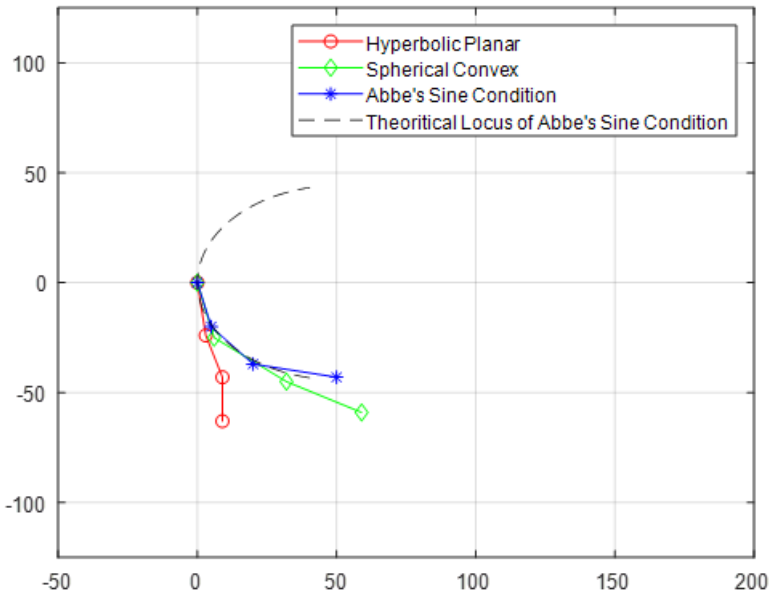

Fig. 11 - Focal points of theoretical and ray tracing results

5. Conclusions

Focal region ray tracing on hyperbolic planar, spherical convex, and Abbe's sine condition lens antenna has been conducted. The feed position is chosen by finding the most concentrated ray points. All lenses show good concentration for 0-degree incident angle. Hyperbolic planar lens shows very distributed ray concentration at incident angle of 10 degrees and above. Spherical convex lens shows better concentrated rays compared to hyperbolic planar lens. However, the focal region is also distorted at incident angle of 10 degrees and above. Abbe's sine condition lens shows very concentrated rays of ray tracing. The ray starts to distort at an incident angle of 30 degrees. Therefore, Abbe's sine condition lens has the best multibeam performance compared to two other lens shapes. Focal region ray tracing results on Abbe's sine condition lens agree well with the theoretical locus. It shows that the proposed focal region ray tracing is correct.

Acknowledgement

Authors are wishing to acknowledge financial support from the Universiti Teknologi Malaysia Prototype Research Grant (UTMPR/PY/2019/02734).

References

[1] Huang, K.-C., & Wang, Z. (2011). Millimeter wave communication systems (Vol. 29): John Wiley & Sons.
[2] Lam, H., Luini, L., Din, J., Alhilali, M., Jong, S., & Cuervo, F. (2017). Impact of rain attenuation on 5G millimeter wave communication systems in equatorial Malaysia investigated through disdrometer data. Paper presented at the 2017 11th European Conference on Antennas and Propagation (EUCAP).
[3] Zhang, J., Huang, Y., Yu, T., Wang, J., & Xiao, M. (2017). Hybrid precoding for multi-subarray millimeter-wave communication systems. IEEE Wireless Communications Letters, 7(3), 440-443.
[4] Alnoman, A., & Anpalagan, A. (2017). Towards the fulfillment of 5G network requirements: technologies and challenges. Telecommunication Systems, 65(1), 101-116.

[5] Hong, W., Jiang, Z. H., Yu, C., Zhou, J., Chen, P., Yu, Z., Jiang, M. (2017). Multibeam antenna technologies for 5G wireless communications. IEEE Transactions on Antennas and Propagation, 65(12), 6231-6249.
[6] Jiang, D., & Liu, G. (2017). An overview of 5G requirements. 5G Mobile Communications, 3-26.
[7] Akyildiz, I. F., Kak, A., & Nie, S. (2020). 6G and beyond: The future of wireless communications systems. IEEE Access, 8, 133995-134030.
[8] Ansarudin, F., Abd Rahman, T., Yamada, Y., Rahman, N. H. A., & Kamardin, K. (2020). Multi beam dielectric lens antenna for 5g base station. Sensors, 20(20), 5849.
[9] Guo, Y., Li, Y., Wang, J., Ge, L., Zhang, Z., Chen, M., He, R. (2021). A 3d printed nearly isotropic luneburg lens antenna for millimeter-wave vehicular networks. IEEE Transactions on Vehicular Technology, 71(2), 1145-1155.
[10] Saleem, M. K., Vettikaladi, H., Alkanhal, M. A., & Himdi, M. (2017). Lens antenna for wide angle beam scanning at 79 GHz for automotive short range radar applications. IEEE Transactions on Antennas and Propagation, 65(4), 2041-2046.
[11] Lo, Y. T., & Lee, S. (2013). Antenna Handbook: theory, applications, and design: Springer Science & Business Media.
[12] Yousuke, T., Yamada, Y., Sasaki, S., & Kezuka, A. (2004). Calculation of wide angle radiation patterns and caustics of a dielectric lens antenna by a ray tracing method. IEICE transactions on electronics, 87(9), 1432-1440.
[13] Van Hung, P., Dinh, N. Q., Dung, D. T., & Yamada, Y. (2020). Caustics and Beam Steering Calculations of Negative Refractive Index Lens Antenna by the Ray Tracing Method. Paper presented at the 2020 International Conference on Advanced Technologies for Communications (ATC).
[14] Muhsin, M., Kamardin, K., & Yamada, Y. (2022). Focal Region Ray Tracing of Dielectric Lens Antennas for Multibeam Designing. Paper presented at the 2022 International Symposium on Antennas and Propagation (ISAP).
[15] Silver, S. (1984). Microwave antenna theory and design: Iet.
[16] Bryant, F. (1958). Snell's law of refraction. Physics Bulletin, 9(12), 317.